Materials and Design 86 (2015) 598–602

Contents lists available at ScienceDirect

Materials and Design

journal homepage: www.elsevier.com/locate/jmad

High strain-rate compressive deformation behavior of the $Al_{0.1}CrFeCoNi$ high entropy alloy

N. Kumar [a], Q. Ying [b], X. Nie [b], R.S. Mishra [a,*], Z. Tang [c], P.K. Liaw [c], R.E. Brennan [d], K.J. Doherty [d], K.C. Cho [d]

[a] Center for Friction Stir Processing, Department of Materials Science and Engineering, University of North Texas, Denton, TX 76203, USA
[b] Department of Mechanical and Energy Engineering, University of North Texas, Denton, TX 76203, USA
[c] Department of Materials Science and Engineering, The University of Tennessee, Knoxville, TN 37996, USA
[d] Weapons and Materials Research Directorate, U.S. Army Research Laboratory, Aberdeen Proving Ground, MD 21005, USA

ARTICLE INFO

Article history:
Received 5 June 2015
Received in revised form 28 July 2015
Accepted 29 July 2015
Available online 30 July 2015

Keywords:
High entropy alloy
High strain-rate deformation
Twinning
Work hardening
Mechanical property
Split Hopkinson pressure bar

ABSTRACT

High entropy alloy is a new class of structural metallic materials. No work, so far, has been carried-out to understand high strain-rate plastic deformation behavior and resulting microstructure. This work focuses on understanding the deformation behavior of an $Al_{0.1}CrFeCoNi$ HEA at high strain-rate (HSR). HSR plastic deformation in compression mode was carried out using split-Hopkinson pressure bar. The pre- and post-deformation microstructures were studied using electron microscopes. A high strain-rate sensitivity of yield strength, significant work hardening, and profuse twinning are main characteristics observed during deformation of the alloy at HSR. Overall, the deformation behavior of the alloy was consistent with low stacking fault energy materials.

1. Introduction

High entropy alloys (HEAs) are multi-component systems that derive their name from the high configurational entropy they possess [1]. Mechanical properties such as hardness, strength (room and high temperatures), ductility, fatigue, and fracture toughness have been reported to be either comparable or better than conventional metallic materials [1–9]. It has caused a surge in research activities on many fronts including fundamentals of plastic deformation behavior of HEAs [1].

The reported research so far has focused on understanding plastic deformation behavior of HEAs at quasi-static strain-rates under temperatures ranging from cryogenic to high temperatures, predominantly in compression mode [1]. Initial reports on mechanical properties of HEAs consisted of microhardness data and/or data from uniaxial compression testing [1]. Moreover, majority of the alloys tested in compression mode were either multiphase alloys or single phase alloys having body-centered cubic (BCC) crystal structure [11–21]. These HEAs were tested in compression due to limited tensile ductility. In recent years, a few reports have appeared on tensile deformation behavior of HEAs [2–7,10]. All the alloys tested in uniaxial tension mode have face-centered cubic (FCC) crystal structure. However, there are only a few reports which have dealt with mechanical properties in compression mode of single phase FCC HEAs [22–25].

The micro-mechanisms of plastic deformation are known to be strain-rate dependent and understanding of high strain-rate (HSR) plastic deformation behavior is also critical for structural applications. Tong et al. [25] have studied mechanical performance of high entropy alloy $Al_xCoCrCuFeNi$ up to 10 s^{-1} and above 300 °C (573 K). However, at present, there is no work reported on very high strain-rate plastic deformation behavior of HEAs. The scope of the present work is to study plastic deformation behavior and deformed microstructure of an HEA at HSR in compression. The HSR deformation behavior of $Al_{0.1}CrFeCoNi$ will be compared with the plastic deformation behavior of the alloy carried out in quasi-static condition in compression mode.

2. Materials and methods

In the present study, a single phase face-centered cubic (FCC) $Al_{0.1}CrFeCoNi$ HEA (Fig. 1(a)) was used to study plastic deformation behavior at HSR. A split-Hopkinson pressure bar was used to deform the alloy at HSR. To ensure dynamic stress equilibrium and constant strain-rate plastic deformation, a mild steel pulse shaper, 1.5 mm in thickness and 8.7 mm in diameter, was used during testing at the impact loading end of the incident bar. Moreover, a single-loading technique was used to avoid reloading of the sample. A $3 \times 3 \times 3$ mm^3 sample was deformed in compression at a strain-rate of ~1000 s^{-1} and ~2600 s^{-1}. The HSR results were compared with the samples tested in compression under quasi-static testing conditions (at strain rates of 10^{-3}, 10^{-2} and 10^{-1} s^{-1}). The samples used in the quasi-

* Corresponding author.
E-mail address: Rajiv.Mishra@unt.edu (R.S. Mishra).

http://dx.doi.org/10.1016/j.matdes.2015.07.161
0264-1275/

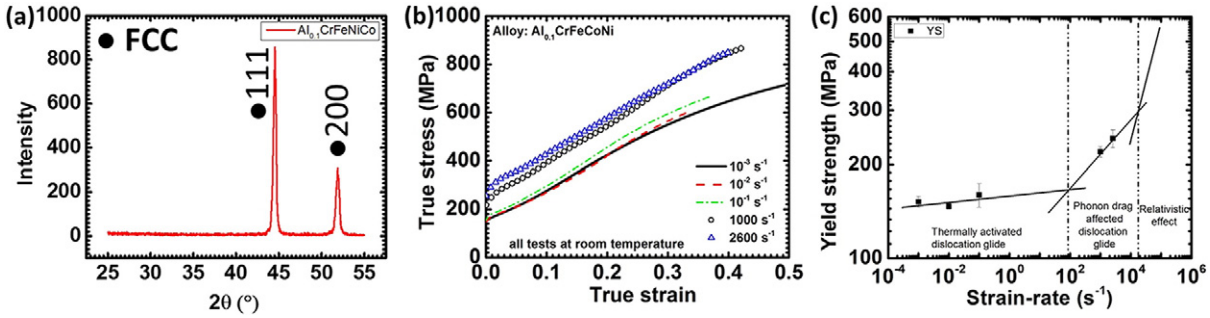

Fig. 1. (a) XRD result showing single phase and FCC structure, (b) True stress– true strain curves at different strain rates, and (c) plot showing yield strength variation as a function of strain-rate and deformation mechanisms in different regimes.

static compression test had the same dimensions as the samples used for the HSR compression test (at least three samples at each strain-rate), and all the tests were conducted at room temperature. All the tests in compression were done only up to the plastic strains shown in Fig. 1(b). Microstructural characterization was carried out using scanning electron microscopy (SEM), electron backscattered diffraction (EBSD), and transmission electron microscopy (TEM) for as-received samples and samples deformed at 10^{-3} and ~2600 s^{-1} strain-rates.

3. Results and discussion

Fig. 1(b) shows the true stress (σ)–true strain (ε) curves for the samples tested in compression under quasi-static and HSR testing conditions. The average yield stress (YS) was 152 ± 6, 147 ± 3, 160 ± 14 MPa for the alloy tested at 10^{-3}, 10^{-2}, and 10^{-1} s^{-1} strain-rates, respectively, and 220 ± 9 and 243 ± 16 MPa for the alloy tested at ~1000 and ~2600 s^{-1}, respectively. Evidently, the YS of the alloy tested in quasi-static condition showed a low strain-rate dependence. However, a strong strain-rate dependence of YS for the samples tested at high strain-rates can be noted here. Although there is scarcity of mechanical property data for HEA with FCC crystal structure tested in compression mode, the reported values of yield strength and extent of work hardening, in literature, are similar to the one observed for $Al_{0.1}$CrFeCoNi alloy in the present work. For example, Wang et al. [22] have carried out compression testing of CoCrCuFeNi HEA, and yield strength was found to be 230 MPa. At about 50% true plastic strain the flow stress reached 890 MPa which is suggestive of high strain hardening behavior of the CoCrCuFeNi HEA. In another report, Salishchev et al. [23] found yield strength of CoCrFeNi alloy to be 190 MPa. Overall, yield strength values demonstrated by single phase FCC HEAs are small as compared to that exhibited by single phase BCC alloys.

The imposed strain-rate ($\dot{\varepsilon}$) and dislocation velocity are related by: $\dot{\varepsilon} = \rho b v$, where ρ, b, and v are the dislocation density, Burgers vector, and dislocation velocity, respectively. Dislocation velocity is related to the applied stress by: $v = K\sigma^p$, where K and p are constants. Replacing v in strain rate–dislocation velocity relationship with $v = K\sigma^p$ results in: $\dot{\varepsilon} = \rho b K \sigma^p$. Rearranging the terms of this expression results in the following expression: $\sigma = A\dot{\varepsilon}^{1/p}$. In this expression parameter A combines other variables mentioned in the equations before. Fig. 1(c) shows a plot between σ and $\dot{\varepsilon}$ on log–log scale depicting three fundamental regions — thermally activated dislocation glide (I), phonon drag (II), and relativistic effect (III) regions [26]. Note in Fig. 1(c) a significantly higher slope (~0.10) in phonon drag regime compared to the slope of 0.01 of the linear regime in thermally activated region — a 10-fold difference in the slope between these two regions. Based on literature [26], the strain-rate dependence of flow stress in region I is expected to be low. The large jump in YS at HSR is probably due to phonon drag effect on the motion of dislocations.

Dislocation velocities are very small for the tests carried out in quasi-static conditions. Hence dislocations interact with an isotropic flux of phonons from surrounding regions and phonon drag has negligible influence on the dislocation motion. In such situations the YS changes at slow rate with a change in strain-rate and that is mostly due to a dependence of thermally activated obstacles on strain-rates. However, at HSR dislocation velocities are so high that phonon drag on dislocation motion is no more negligible. Due to which we see a pronounced effect of strain-rate change on YS in HSR deformation regime as shown in Fig. 1(c) [26]. Note that the third regime 'relativistic effect' has been drawn schematically based on information in literature [26]. In this regime the dislocation velocity start approaching shear wave velocity. But the velocity is considered to be less than shear wave velocity because of shear strain (or stress) fields associated around dislocations. It starts becoming effective at dislocation wave velocities of 0.8 C_s, where C_s is shear wave velocity. In terms of strain-rate, such a high velocity of dislocation corresponds to strain-rate of ~10^4 s^{-1} or higher. Such a high level of strain-rate can be achieved during shock loading of materials and requires the flow stress to rise rapidly to make dislocations move at a strain-rate comparable to externally imposed strain-rates.

The alloy tested in both conditions showed significant work hardening — the flow stress increased from ~150–250 MPa upon yielding to ~700–870 MPa at the end of plastic strain 0.4–0.5 (Fig. 1(b)). Such a high level of work hardening has been demonstrated by SS304 and Inconel 718 [27,28]. However, note that although the alloys such as SS304 and Inconel 718 are compositionally complex, they possess many phases which assist in work hardening. Despite being a single phase alloy, the similar work hardening behavior in this HEA is remarkable.

The work hardening behavior of the alloy is further analyzed by plotting the variation of work hardening rate as a function of true plastic strain (Fig. 2(a)) and with flow stress (Fig. 2(b)). Both plots show a change in the slope of strain hardening rate (dσ/dε) as deformation proceeds. Overall, three different regimes should be noted in the dσ/dε vs. ε/σ curves in Fig. 2 — a curve having a negative slope followed by a positive slope region which is again followed by a negative slope region at higher plastic strain or flow stress. Such transitions are reported to be due to a change in the deformation mechanism — region I: dislocation-slip-dominated plastic deformation, region II: twinning-dominated plastic deformation, and region III: dislocation-slip-dominated plastic deformation [29]. For the sample tested in quasi-static and HSR conditions, the slope of the curve changed from negative (region I) to positive (region II) after a plastic strain ($\varepsilon_{I/II}$) of ~0.042 ± 0.011 and ~0.050 ± 0.010, respectively. The rise in flow stress ($\sigma_{I/II} - \sigma_y$) after yielding was 54 ± 15 MPa for the sample tested under quasi-static conditions ($\sigma_{I/II}$ is the flow stress at transition from regions I to II) and for HSR samples 120 ± 24 MPa. This suggests that the critical plastic strain and stress for the onset of twin nucleation increases for the alloy tested at HSR.

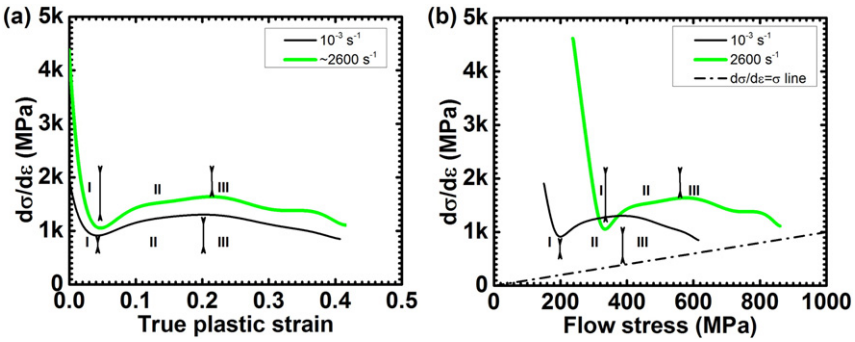

Fig. 2. (a) Work hardening rate (dσ/dε) vs. true plastic strain plot and (b) Kocks–Mecking plot showing variation of dσ/dε as a function of true stress.

The onset of region III at HSR (~2600 s^{-1}) occurred at a true strain of ~0.2 for the sample shown in Fig. 2(a). However, for other two samples tested at HSR it was difficult to determine the start of region III due to undulation in the strain hardening rate curves after stage I. For the samples tested under quasi-static condition (~10^{-3} s^{-1}) the onset of region III took place at an average plastic strain of 0.173 ± 0.036.

As noted earlier, the sample tested at HSR showed a YS at least about 60 MPa higher than the deformed sample tested at low strain-rates. This type of YS dependence on strain-rate is typical of low stacking fault (SF) energy materials. For example, Lee and Lin [26] have studied the HSR plastic deformation behavior of 304 L stainless steel (SS). A similar dependence of YS, as reported here, on strain-rate was reported by the same researchers in 304 L SS. In another alloy, the nitrogen-alloyed austenitic stainless steel, Fréchard et al. [30] noted a similar trend for YS as a function of strain-rate. A careful comparison revealed that all alloys which showed strong dependence of YS on strain-rate had low SF energy [27,28,30]. A study carried out on Cu-*x* (wt%)Al (*x* = 0.2, 2, 4, and 6) by Rohatgi et al. [29] provides evidence of the role of SF energy on YS as a function of strain-rate.

It is known that phonon drag phenomenon becomes very effective during plastic deformation at HSR such as in the present case [26]. Hence, a phonon drag mechanism might be operative at HSR based on the significant rise in YS. It is based on the argument that in this domain, higher shear stress is required to increase the dislocation velocity necessary for the imposed strain-rate. Additionally, Ferreira et al. [31] have suggested that dislocation partials are more active at HSR to match the imposed strain-rate. It was argued that due to a lower jump frequency, perfect dislocations are unable to move at a velocity required to make the internal strain-rate equal to the imposed strain-rate, and partial dislocations are much more suited under such experimental conditions. Zaddach et al. [32] have investigated the stacking-fault energy (SFE) of CrFeCoNi and CrMnFeCoNi alloys. The SFE of these alloys were found to lie between 20 and 30 mJ/m^2. With addition of Al in CrFeCoNi the SFE is expected to decrease further. Hence, it will be reasonable to assume that $Al_{0.1}$CrFeCoNi has very small SFE (lower than CrFeCoNi). The work of Rohatgi et al. [29] also shows that the addition of Al to Cu caused a decrease in SFE of Cu. Hence, based on the assumption of low stacking fault energy of the HEA used in the present study, it is likely that dislocation glide on the slip planes takes place due to movement of dislocation partials that are much more active at HSR. Hence, it is possible that phonon drag and high propensity of dislocation partials caused such a significant rise in YS at high strain-rate.

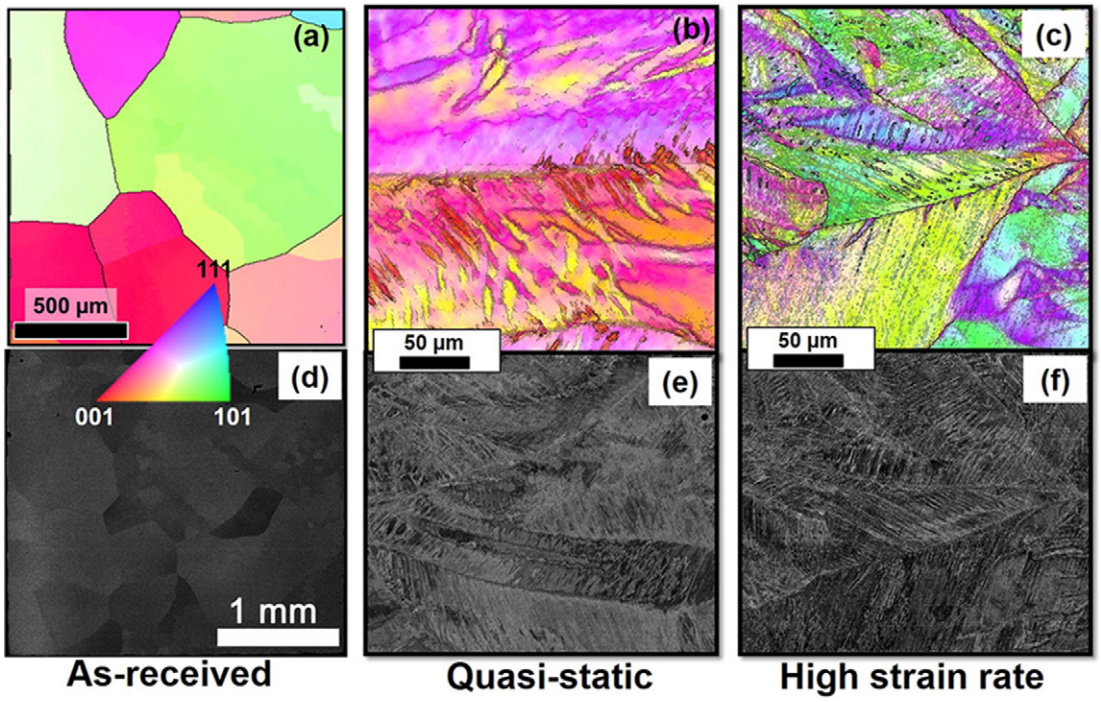

Fig. 3. Electron backscatter diffraction images (a)–(c) and scanning electron microscope (d)–(f) images for as-received (a, d) and deformed samples — quasi-static (10^{-3} s^{-1}): (b, e), high strain-rate (~2600 s^{-1}): (c, f).

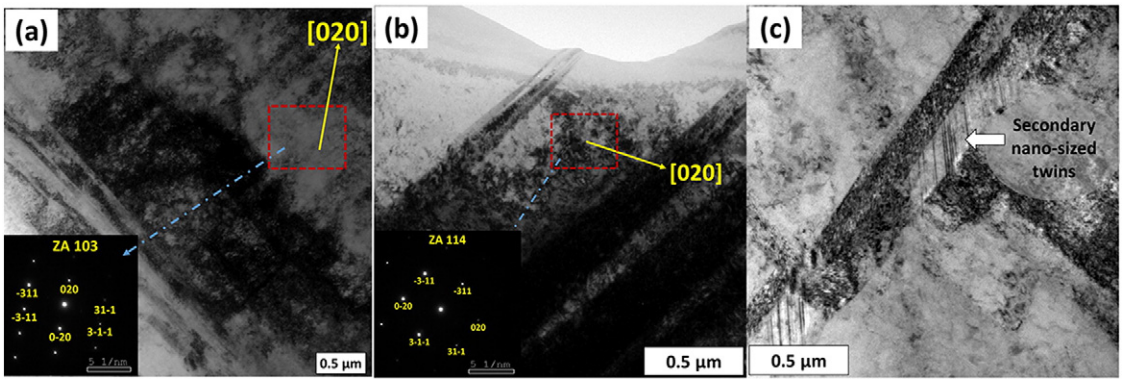

Fig. 4. TEM images showing different microstructural features in the deformed samples; (a) quasi-statically deformed (10^{-3} s^{-1}), ZA [103] and (b) & (c) deformed at high strain-rate (~2600 s^{-1}) (b) [ZA 114] and (c) away from zone axis and in multi-beam condition.

The SEM and the EBSD images for the alloy in different conditions are shown in Fig. 3. It is evident that the alloy in the as-received condition consists of grains on the order of millimeters in size (Fig. 3(a) and (d)). Both deformed samples showed profuse twinning. The SEM images shown in Fig. 3(e) and (f) are electron channeling contrast images taken on a polished surface in backscatter electron imaging mode. A visual comparison of Fig. 3(e) and (f) suggests a higher twin density in the sample deformed at HSR compared to the sample deformed at quasi-static condition. A similar set of observation can be made from the comparison of Fig. 3(b) and (c). Note that in FCC metals and alloys, twinning takes place by shear of atoms on {111} planes along a/6 < 112 > direction.

Twinning is a dominant mode of plastic deformation in alloys having low SF energy [31]. Work hardening during the quasi-static plastic deformation after an average plastic strain of 0.042 can be attributed mainly to dislocation–twin boundary interactions. Just as in other systems, the rise in the work hardening rate is also expected to be due primarily to an increase in twin density with increase in flow stress. For the sample deformed at HSR, the rise in strain hardening rate due to dislocation–twin boundary interaction is found to begin after an average plastic strain of 0.05 was reached (Fig. 2(a)). It should be noted here that although the rise in flow stress of the HEA alloy was similar to SS 304 and Inconel 718, the work hardening behavior of the HEA alloy was different, as SS304 and Inconel 718 did not show the presence of region II [27,28]. Note that the SF energy of SS 304 is ~25 mJ/m^2 [14]. The presence of region II, similar to the one exhibited by the present alloy, can be noted in the work of Rohatgi et al. [29] on compressively deformed Cu–6 wt.%Al under quasi-static conditions. The SF energy of Cu–6 wt.%Al is reported to be between 4 and 7 mJ/m^2. Rohatgi et al. [29] also showed that Cu–Al alloys with SF energies greater than Cu–6 wt.%Al, the slope of region II was lower than regions I and III and in some cases an absence of region II. Hence, it appears that $Al_{0.1}$CrFeCoNi has a very small SF energy, which is causing extensive twinning, and causing the transition from a negative slope in region I to a positive slope in region II in Fig. 2(a) and (b).

SFE and its role in twin formation require some further discussion at this point. The HEA CrMnFeCoNi, which has SFE of ~20 mJ/m^2 as reported by Zaddach et al. [32], did not exhibit twinning at room temperature when tested under uniaxial tensile mode [3]. It is interesting to note that CrFeCoNi alloy has SFE of ~30 mJ/m^2 [32] and even after adding 20 at.% (19.7 wt.%) Mn, the SFE of CrMnFeCoNi alloy decreased only by a very small amount. In contrast, Cu has an SFE of 80 mJ/m^2 [29]. However, just by adding 2.5 wt.% Al to Cu, the SFE decrease from 80 to 37 mJ/m^2 which decreased further down to 4 mJ/m^2 after addition of 8 wt.% of Al to Cu.

It may be associated with larger atomic size difference between Al and other elements in the alloys being discussed here. Hence, addition of Al would cause a high lattice strain per atomic percent in CrFeCoNi as compared to Mn. Mishra et al. [33] have recently suggested that lattice strain in HEA might play an important role in dislocation core energy which in turn will have bearing on stacking fault formation and its energy. Since $Al_{0.1}$CrFeCoNi has ~1.2 wt.% of Al, it may be safely assumed that Al addition might have caused a decrease in SFE from ~30 mJ/m^2 to a lower value. The extent of decrease can only be speculated at this moment based on observation of extensive twinning in compression mode. Based on foregoing discussion and experimental observations, it seems like a stacking fault energy below 20 mJ/m^2 might be needed to promote deformation twinning during plastic deformation.

In addition to a very small value of SFE, another factor which might promote the formation of deformation twins even in alloys having relatively large SFE is mode of deformation. For example, in the work reported by Otto et al. [3], the HEA CrMnFeCoNi didn't show any evidence of deformation twins when deformed in uniaxial tension at room temperature. On the other hand, the HEA $Al_{0.1}$CrFeCoNi alloy investigated in the present study had shown deformation twins under tensile deformation condition [7]. Recently Schuh et al. [34] have shown the presence of high density of deformation twins during plastic deformation of the HEA CrMnFeCoNi alloy under high pressure torsion. Since the $Al_{0.1}$CrFeCoNi HEA showed deformation twins both under tension and compression, we believe that the deformation twins exhibited by the HEA $Al_{0.1}$CrFeCoNi during plastic deformation under uniaxial compression are a consequence of very low SFE.

A bright field (BF) TEM image taken at zone axis (ZA) [103] for the sample deformed at 10^{-3} s^{-1} is shown in Fig. 4(a). A BF TEM image for the sample deformed at ~2600 s^{-1} is shown in Figs. 4(b) (ZA [114]) and 4(c) (away from zone axis). Several sets of parallel bands can be seen in Fig. 4(a). The comparison of these microstructural features from the images reported in the literature suggests that these features are deformation twins. In addition to this, regions of high dislocation density should also be noted in Fig. 4(a). The deformation twins observed for the sample deformed at HSR are shown in Fig. 4(b). Again, it shows several sets of parallel bands. In addition to this, secondary deformation nano-twins are also observed for the sample deformed at HSR, as evident from Fig. 4(c). Such microstructures are also observed in the deformed condition for other alloys having low SF energies [31].

4. Conclusions

In conclusion, the initial investigation of HSR plastic deformation behavior of HEA $Al_{0.1}$CrFeCoNi alloy is suggestive of a deformation behavior similar to low SF materials. The HEA investigated here exhibited high SRS during plastic deformation at HSR compared to those tested in quasi-static regime. The onset of twinning was dependent on the strain-rate, and exceptional work hardening rate was observed irrespective of the strain-rates. Specimens

deformed at HSR exhibited secondary nano-twins that were not observed in quasi-static tested specimens.

Acknowledgments

The work was performed under a cooperative agreement between the Army Research Laboratory and the University of North Texas (W911NF-13-2-0018). The authors are also thankful to the Center for Advanced Research and Technology (CART) for providing access to the microscopy facilities at the University of North Texas.

References

[1] Y. Zhang, T.T. Zuo, Z. Tang, M.C. Gao, K.A. Dahmen, P.K. Liaw, Z.P. Lu, Microstructures and properties of high-entropy alloys, Prog. Mater. Sci. 61 (2014) 1, http://dx.doi.org/10.1016/j.pmatsci.2013.10.001.
[2] J.Y. He, W.H. Liu, H. Wang, Y. Wu, X.J. Liu, T.G. Nieh, Z.P. Lu, Effects of Al addition on structural evolution and tensile properties of the FeCoNiCrMn high-entropy alloy system, Acta Mater. 62 (2014) 105, http://dx.doi.org/10.1016/j.actamat.2013.09.037.
[3] F. Otto, A. Dlouhý, Ch. Somsen, H. Bei, G. Eggeler, E.P. George, The influences of temperature and microstructure on the tensile properties of a CoCrFeMnNi high-entropy alloy, Acta Mater. 61 (2013) 5743, http://dx.doi.org/10.1016/j.actamat.2013.06.018.
[4] T.-T. Shun, Y.-C. Du, Microstructure and tensile behaviors of FCC $Al_{0.3}$CoCrFeNi high entropy alloy, J. Alloys Compd. 479 (2009) 157, http://dx.doi.org/10.1016/j.jallcom.2008.12.088.
[5] M.J. Yao, K.G. Pradeep, C.C. Tasan, D. Raabe, A novel, single phase, non-equiatomic FeMnNiCoCr high-entropy alloy with exceptional phase stability and tensile ductility, Scr. Mater. 72–73 (2014) 5, http://dx.doi.org/10.1016/j.scriptamat.2013.09.030.
[6] N. Kumar, M. Komarasamy, N. Phalgun, Z. Tang, P.K. Liaw, R.S. Mishra, Friction stir processing of a high entropy alloy $Al_{0.\ 1}$CoCrFeNi, JOM 67 (2015) 1007, http://dx.doi.org/10.1007/s11837-015-1385-9.
[7] M. Komarasamy, N. Kumar, Z. Tang, R.S. Mishra, P.K. Liaw, Effect of microstructure on the deformation mechanism of friction stir-processed $Al_{0.1}$CoCrFeNi high entropy alloy, Mater. Res. Lett. 3 (2015) 30, http://dx.doi.org/10.1080/21663831.2014.958586.
[8] M.A. Hemphill, T. Yuan, G.Y. Wang, J.W. Yeh, C.W. Tsai, A. Chuang, P.K. Liaw, Fatigue behavior of Al0.5CoCrCuFeNi high entropy alloys, Acta Mater. 60 (2012) 5723, http://dx.doi.org/10.1016/j.actamat.2012.06.046.
[9] B. Gludovatz, A. Hohenwarter, D. Catoor, E.H. Chang, E.P. George, R.O. Ritchie, A fracture-resistant high-entropy alloy for cryogenic applications, Science 345 (2014) 1153, http://dx.doi.org/10.1126/science.1254581.
[10] L. Liu, J.B. Zhu, L. Li, J.C. Li, Q. Jiang, Microstructure and tensile properties of FeMnNiCuCoSnx high entropy alloys, Mater. Des. 44 (2013) 223, http://dx.doi.org/10.1016/j.matdes.2012.08.019.
[11] J.M. Zhu, H.M. Fu, H.F. Zhang, A.M. Wang, H. Li, Z.Q. Hu, Microstructure and compressive properties of multiprincipal component AlCoCrFeNiCx alloys, J. Alloys Compd. 509 (2011) 3476, http://dx.doi.org/10.1016/j.jallcom.2010.10.047.
[12] J.M. Zhu, H.M. Fu, H.F. Zhang, A.M. Wang, H. Li, Z.Q. Hu, Synthesis and properties of multiprincipal component AlCoCrFeNiSix alloys, Mater. Sci. Eng. A 527 (2010) 7210, http://dx.doi.org/10.1016/j.msea.2010.07.049.
[13] H. Zhang, Y.Z. He, Y. Pan, Y.S. He, K. Shin, Synthesis and characterization of NiCoFeCrAl3 high entropy alloy coating by laser cladding, Adv. Mater. Res. Manuf. Sci. Eng. 97–101 (2010) 1408, http://dx.doi.org/10.4028/www.scientific.net/AMR.97-101.1408.
[14] Y.P. Wang, B.S. Li, M.X. Ren, C. Yang, H.Z. Fu, Microstructure and compressive properties of AlCrFeCoNi high entropy alloy, Mater. Sci. Eng. A 491 (2008) 154, http://dx.doi.org/10.1016/j.msea.2008.01.064.
[15] Y.J. Zhou, Y. Zhang, Y.L. Wang, G.L. Chen, Solid solution alloys of AlCoCrFeNiTix with excellent room-temperature mechanical properties, Appl. Phys. Lett. 90 (2007) 181904, http://dx.doi.org/10.1063/1.2734517.
[16] J.M. Zhu, H.F. Zhang, H.M. Fu, A.M. Wang, H. Li, Z.Q. Hu, Microstructures and compressive properties of multicomponent AlCoCrCuFeNiMox alloys, J. Alloys Compd. 497 (2010) 52, http://dx.doi.org/10.1016/j.jallcom.2010.03.074.
[17] S.G. Ma, Y. Zhang, Effect of Nb addition on the microstructure and properties of AlCoCrFeNi high-entropy alloy, Mater. Sci. Eng. A 532 (2012) 480, http://dx.doi.org/10.1016/j.msea.2011.10.110.
[18] F.J. Wang, Y. Zhang, G.L. Chen, Atomic packing efficiency and phase transition in a high entropy alloy, J. Alloys Compd. 478 (2009) 321, http://dx.doi.org/10.1016/j.jallcom.2008.11.059.
[19] Y.J. Zhou, Y. Zhang, Y.L. Wang, G.L. Chen, Microstructure and compressive properties of multicomponent Al-X(TiVCrMnFeCoNiCu)(100-X) high-entropy alloys, Mater. Sci. Eng. A 454 (2007) 260, http://dx.doi.org/10.1016/j.msea.2006.11.049.
[20] Z.H. Hu, Y.Z. Zhan, G.H. Zhang, J. She, C.H. Li, Effect of rare earth Y addition on the microstructure and mechanical properties of high entropy AlCoCrCuNiTi alloys, Mater. Des. 31 (2010) 1599.
[21] Y.D. Wu, Y.H. Cai, X.H. Chen, T. Wang, J.J. Si, L. Wang, Y.D. Wang, X.D. Hui, Phase composition and solid solution strengthening effect in TiZrNbMoV high-entropy alloys, Mater. Des. 83 (2015) 651, http://dx.doi.org/10.1016/j.matdes.2015.06.072.
[22] X.F. Wang, Y. Zhang, Y. Qiao, G.L. Chen, Novel microstructure and properties of multicomponent CoCrCuFeNiTix alloys, Intermetallics 15 (2007) 357, http://dx.doi.org/10.1016/j.intermet.2006.08.005.
[23] G.A. Salishchev, M.A. Tikhonovsky, D.G. Shaysultanov, N.D. Stepanov, A.V. Kuznetsov, I.V. Kolodiy, A.S. Tortika, O.N. Senkov, Effect of Mn and V on structure and mechanical properties of high-entropy alloys based on CoCrFeNi system, J. Alloys Compd. 591 (2014) 11, http://dx.doi.org/10.1016/j.jallcom.2013.12.210.
[24] N.D. Stepanov, D.G. Shaysultanov, N.Y. Yurchenko, S.V. Zherebtsov, A.N. Ladygin, G.A. Salishchev, M.A. Tikhonovsky, High temperature deformation behavior and dynamic recrystallization in CoCrFeNiMn high entropy alloy, Mater. Sci. Eng. A 636 (2015) 188, http://dx.doi.org/10.1016/j.msea.2015.03.097.
[25] C.-J. Tong, M.-R. Chen, J.-W. Yeh, S.-J. Lin, S.-K. Chen, T.-T. Shun, S.-Y. Chang, Mechanical performance of the AlxCoCrCuFeNi high-entropy alloy system with multiprincipal elements, Metall. Mater. Trans. A 36 (2005) 1263, http://dx.doi.org/10.1007/s11661-005-0218-9.
[26] M.A. Meyers, Dynamic Behavior of Materials, John Wiley & Sons, 1994.
[27] W. Lee, C. Lin, Comparative study of the impact response and microstructure of 304 L stainless steel with and without prestrain, Metall. Mater. Trans. A 33 (2002) 2801, http://dx.doi.org/10.1007/s11661-002-0265-4.
[28] W. Lee, C. Lin, T. Chen, H. Chen, Dynamic mechanical behaviour and dislocation substructure evolution of Inconel 718 over wide temperature range, Mater. Sci. Eng. A 528 (2011) 6279, http://dx.doi.org/10.1016/j.msea.2011.04.079.
[29] A. Rohatgi, K. Vecchio, G.T. Gray III, The influence of stacking fault energy on the mechanical behavior of Cu and Cu–Al alloys: deformation twinning, work hardening, and dynamic recovery, Metall. Mater. Trans. A 32 (2001) 135, http://dx.doi.org/10.1007/s11661-001-0109-7.
[30] S. Fréchard, A. Redjaïmia, E. Lach, A. Lichtenberger, Dynamical behaviour and microstructural evolution of a nitrogen-alloyed austenitic stainless steel, Mater. Sci. Eng. A 480 (2008) 89, http://dx.doi.org/10.1016/j.msea.2007.07.014.
[31] P. Ferreira, J. Vander Sande, M.A. Fortes, A. Kyrolainen, Microstructure development during high-velocity deformation, Metall. Mater. Trans. A 35 (2004) 3091, http://dx.doi.org/10.1007/s11661-004-0054-3.
[32] A.J. Zaddach, C. Niu, C.C. Koch, D.L. Irving, Mechanical properties and stacking fault energies of NiFeCrCoMn high-entropy alloy, JOM 65 (2013) 1780, http://dx.doi.org/10.1007/s11837-013-0771-4.
[33] R.S. Mishra, N. Kumar, M. Komarasamy, Lattice strain framework for plastic deformation in complex concentrated alloys including high entropy alloys, Mater. Sci. Technol. 31 (2015) 1259, http://dx.doi.org/10.1179/1743284715Y.0000000050.
[34] B. Schuh, F. Mendez-Martin, B. Völker, E.P. George, H. Clemens, R. Pippan, A. Hohenwarter, Mechanical properties, microstructure and thermal stability of a nanocrystalline CoCrFeMnNi high-entropy alloy after severe plastic deformation, Acta Mater. 96 (2015) 258, http://dx.doi.org/10.1016/j.actamat.2015.06.025.